Medicinal Plant Biology

ARTICLE

Open Access

https://doi.org/10.48130/mpb-0025-0040

Medicinal Plant Biology **2026**, 5: e002

Comprehensive genome-wide identification and functional characterization of non-specific lipid transfer proteins in *Artemisia annua* L.

Hangyu Wen[1#], Wei Wang[1,2#], Weizhi He[1], Hang Liu[1], Lei Su[1], Xinyi Hu[1], Xin Yan[1], Bowen Peng[1], Yaojie Zhang[1], Pin Liu[1], Shouchao Yan[3], Eddie Wu[1], Xueqing Fu[1], Li Ren[4], Kexuan Tang[1] and Ling Li[1*]

[1] *Joint International Research Laboratory of Metabolic & Developmental Sciences, Key Laboratory of Urban Agriculture (South) Ministry of Agriculture, Plant Biotechnology Research Center, Fudan-SJTU-Nottingham Plant Biotechnology R&D Center, School of Agriculture and Biology, Shanghai Jiao Tong University, Shanghai 200240, China*

[2] *Center for Plant Biology, School of Life Sciences, Tsinghua University, Beijing 100084, China*

[3] *Department of Biochemistry and Metabolism, John Innes Centre, Norwich Research Park, Norwich NR4 7UH, UK*

[4] *Institute for Agri-Food Standards and Testing Technology, Shanghai Academy of Agricultural Sciences, Shanghai 201403, China*

[#] Authors contributed equally: Hangyu Wen, Wei Wang

[*] Correspondence: liling@sjtu.edu.cn (Li L)

Abstract

Plant non-specific lipid transfer proteins (nsLTPs) are small secretory proteins that bind and transport hydrophobic molecules. nsLTPs are crucial players in various plant physiological processes, including lipid metabolism and defense. In *Artemisia annua*, glandular trichomes serve as the primary sites for artemisinin biosynthesis and storage. Although several nsLTPs have been reported in *Artemisia annua*, a comprehensive genome-wide analysis was previously lacking. In this study, 55 *nsLTP* genes were identified in the *A. annua* genome and classified into eight types (I, II, III, IV, V, VI, VII, and IX) through phylogenetic analysis. Notably, expression profiling revealed that certain *AaLTP* genes, especially *AaLTP1* and *AaLTP2*, exhibit glandular trichome-specific expression, as confirmed by promoter::GUS assays. Overexpression of *AaLTP1* significantly increased artemisinin content by 1.5-fold ($p < 0.05$), suggesting its direct role in facilitating artemisinin accumulation. Furthermore, an HD-ZIP transcription factor, AaHD8, was confirmed as a positive regulator of *AaLTP1* and *AaLTP2* through direct promoter binding. Overall, this study provides the first comprehensive characterization of the *nsLTP* gene family in *A. annua* and establishes a functional link between nsLTPs, glandular trichome biology, and artemisinin biosynthesis, offering new insights for metabolic engineering to enhance artemisinin production.

Citation: Wen H, Wang W, He W, Liu H, Su L, et al. 2026. Comprehensive genome-wide identification and functional characterization of non-specific lipid transfer proteins in *Artemisia annua* L.. *Medicinal Plant Biology* 5: e002 https://doi.org/10.48130/mpb-0025-0040

Introduction

A. annua is an important natural source of artemisinin, a sesquiterpene lactone that forms the backbone of frontline antimalarial therapies[1]. This compound is both synthesized and accumulated predominantly within the glandular secretory trichomes (GSTs)[2]. While metabolic pathways and key enzymes involved in artemisinin biosynthesis have been extensively characterized[3–5], the mechanisms governing the intracellular transport and secretion of hydrophobic intermediates (e.g., dihydroartemisinic acid) within GSTs remain poorly understood. Non-specific lipid transfer proteins (nsLTPs), which facilitate the binding and transport of lipophilic molecules, represent promising candidates for mediating these processes[6]. However, despite their potential roles in secondary metabolite trafficking and stress adaptation, the *nsLTP* family in *A. annua* has not been systematically investigated.

Plant non-specific lipid transfer proteins (nsLTPs) are a group of small secretory proteins in plants that are responsible for transferring phospholipids from liposomes to mitochondria or chloroplasts[6]. All known plant nsLTPs are synthesized as precursors with N-terminal signal peptides. Mature proteins are typically small, with molecular weights usually below 10 kDa[7], and feature a characteristic eight-cysteine motif (ECM) formed by eight cysteine residues arranged as C-Xn-C-Xn-CC-Xn-CXC-Xn-C-Xn-C[8]. The ECM is stabilized by four disulfide bonds, which maintain the three-dimensional structure of the hydrophobic cavity. Various lipids and hydrophobic compounds were shown to bind this structure via *in vitro* assays[9].

nsLTPs were initially thought to be involved in membrane biosynthesis and regulation of intracellular fatty acid pools due to their ability to transfer lipid molecules and bind acyl chains *in vitro*[7]. However, the presence of N-terminal signal peptides in all *nsLTP* precursors suggests their involvement in the secretory pathway. In *Arabidopsis*, LTPG, a glycosylphosphatidylinositol-anchored lipid transfer protein, is highly expressed in the epidermis of inflorescence stems. It primarily localizes to the plasma membrane, binds lipid probes *in vitro*, and may play a role in lipid transport in the cuticle. Reduced wax deposition in the stem cuticle was observed in *ltpg* mutants[10]. Current research has proposed multiple physiological functions for nsLTPs, including plant signaling[11,12], cuticle and wax metabolism[13], cell wall extension[14], pollen development[15–17], somatic embryogenesis[18,19], seed germination[20], response to biotic stresses[21,22] and abiotic stresses[23–26]. For example, nsLTPs have been shown to mediate responses to pathogen attack by interacting with various plant defense pathways[27], while their roles in drought and salinity stress tolerance have been demonstrated through their ability to modulate lipid signaling and cell membrane integrity[28–30]. Nevertheless, a genome-wide analysis of nsLTPs in *A. annua* is lacking, leaving their roles in artemisinin biosynthesis unresolved.

Previous work in *A. annua* identified only four nsLTPs (*AaLTP1–4*), with functional studies limited to heterologous expression systems. *AaLTP1*, *AaLTP*2, and *AaLTP3* have been shown to enhance the accumulation of (DH)AA in the apoplast of *Nicotiana benthamiana* leaves, while *AaLTP3* and *AaLTP4* are involved in sesquiterpene lactone secretion from glandular trichomes in *A. annua*[31]. However, these studies did not address whether nsLTPs directly influence artemisinin biosynthesis in planta or how their expression is regulated. Moreover, the recent release of the *A. annua* genome provides an opportunity to comprehensively characterize the *nsLTP* family and uncover trichome-specific isoforms with specialized roles in artemisinin metabolism[32].

Here, this study addresses these gaps through a genome-wide identification and functional analysis of nsLTPs in *A. annua*. The objectives were to: (1) systematically classify the *nsLTP* family; (2) identify isoforms preferentially expressed in glandular trichomes; (3) validate roles in artemisinin biosynthesis; and (4) elucidate upstream regulatory mechanisms. This study performed a genome-wide analysis of the *nsLTP* gene family, identifying 55 *nsLTP* genes in *A. annua* and classifying them into eight types. Protein structures, chemical characteristics, structural motifs, subcellular localization, evolutionary patterns, and expression profiles were examined. Specifically, two *AaLTP* genes, *AaLTP1* and *AaLTP2*, were cloned and confirmed to exhibit glandular trichome-specific expression. The homeodomain–leucine zipper (HD-Zip) proteins participate in various critical physiological processes, including transcriptional regulation of epidermal and sub-epidermal cell formation, anthocyanin accumulation, wax synthesis, lipid transport, and response to drought signals[33,34]. Interestingly, *AaLTP1* and *AaLTP2* were discovered to be positively regulated by *AaHD8*. Moreover, overexpression of *AaLTP1* reveals a positive role in artemisinin production. This study provides a comprehensive understanding of the *nsLTP* gene family in *A. annua*, highlighting structural and functional diversity, evolutionary aspects, and regulatory mechanisms, particularly in relation to glandular trichome biology and artemisinin biosynthesis.

Materials and methods

Plant materials

The high artemisinin variety 'Hu-Hao 1' of *A. annua* L., derived from Chongqing and further developed over several years in Shanghai, is used in all experiments related to *A. annua*[35,36]. For *in vitro* culture, *A. annua* seeds are initially surface-sterilized by immersion in 70% ethanol for 3 min, followed by washing three times with sterile water. Subsequently, the seeds are sterilized in a 20% sodium hypochlorite solution for 10 min and rinsed five times with sterile water. These sterilized seeds are then sown on MS medium containing 3% sucrose and 0.6% agar (pH = 5.7). *A. annua* plants are grown in pots at a temperature of 23 ± 2 °C under a photoperiod of 16 h light and 8 h darkness[37].

Identification and bioinformatics analysis

The protein data of *A. annua* were obtained from the NCBI database (www.ncbi.nlm.nih.gov/genome) (taxonomic ID: 35608). The HMMER-3.2.1 software (www.hmmer.org) was used to identify proteins containing the LTP domain (accession: PF00234) (plant lipid transfer/seed storage/trypsin-alpha amylase inhibitor). The web tool SignalP 5.0 (https://services.healthtech.dtu.dk/services/SignalP-5.0) was employed to predict mature proteins. Sequences longer than 120 amino acids in mature proteins were discarded, and the presence of ECM was manually checked. The remaining candidate proteins were further confirmed for the LTP domain using the batch Web CD-Search tool (www.ncbi.nlm.nih.gov/Structure/cdd/wrpsb.cgi). The molecular weight and isoelectric point (pI) of *AaLTP* were calculated using the compute pI/Mw tool (https://web.expasy.org/compute_pi). The subcellular localization of *AaLTP* was predicted using DeepLoc-1.0 (www.cbs.dtu.dk/services/DeepLoc-1.0/index.php)[38]. Motif analysis was performed using MEME (https://meme-suite.org/meme/tools/meme). Promoter analysis was conducted using PlantPAN 3.0 (https://plantpan.itps.ncku.edu.tw/plantpan4/promoter_analysis.php). The three-dimensional structure of *AaLTP* was predicted using Phyre2 (www.sbg.bio.ic.ac.uk/phyre2/html)[39]. The coding sequence of the *AaLTP* gene is shown in Supplementary Table S1.

Alignment and phylogenetic analysis

Protein sequences of *A. annua* and *A. thaliana* were downloaded from NCBI (www.ncbi.nlm.nih.gov) and TAIR (www.arabidopsis.org), respectively. Multiple sequence alignment of the ECM domain was performed using MAFFT and manually adjusted[40]. The results of the multiple sequence alignment were visualized using Jalview software. Using MEGA 7.0 software, maximum likelihood phylogenetic trees were constructed for *A. annua* under the Complete deletion and LG + G + I model, and for *A. annua* and *A. thaliana* under the Complete deletion and WAG + G + I model[41]. To validate reliability, 1,000 bootstrap replicates were performed. The above-mentioned best-fit model was selected using the 'Find Best DNA/Protein Models' function built into MEGA 7.0, with parameters set to 'Complete deletion' for gap treatment and 'Very Strong' for the branch swap filter to ensure the highest accuracy. Further tree beautification was done using iTOL (http://itol.embl.de) and Figtree software.

Expression analysis of nsLTPs

RPKM (Reads Per Kilobase of gene model per Million) values of AaLTPs in various organs (root, stem, leaf, seed, bud, and trichome) were extracted from RNA-seq data of *A. annua* (SRP129502)[42]. TPM (Transcripts Per Kilobase Million) values of all differentially expressed genes (DEGs) from *AaHD8*-RNAi lines were extracted from RNA-seq data (Supplementary Table S2)[43]. Subsequently, differential expression analysis of different organs and *AaHD8*-RNAi lines was performed using the online tool imageGP (www.ehbio.com/ImageGP/index.php).

Cloning procedures and transformation

The full-length coding sequences of *AaLTP1* and *AaLTP2* were amplified from *A. annua* cDNA using primers LTP1-F/R and LTP2-F/R, respectively, with engineered *BamH* I and *Xba* I restriction sites flanking both sequences. Following sequencing verification, the digested PCR products were directionally cloned into the PHB plant expression vector to generate EYFP fusion constructs under the control of the CaMV35S promoter, yielding recombinant plasmids pHB-AaLTP1 and pHB-AaLTP2. For promoter activity analysis, the upstream regulatory regions of *AaLTP1* and *AaLTP2* were amplified using primers listed in Supplementary Table S3 and cloned into the pCambia 1391Z vector to drive GUS expression.

All constructs (pHB-AaLTP1, pHB-AaLTP2, and promoter-GUS fusions) were introduced into *Agrobacterium tumefaciens* strain EHA105 via electroporation. *A. annua* leaf explants were transformed using established Agrobacterium-mediated methods[44]. For overexpression studies, transgenic lines harboring pHB-AaLTP1

or pHB-AaLTP2 were screened by PCR amplification of genomic DNA using primers spanning the vector-AaLTP junctions. For GUS assays, plants transformed with promoter-GUS constructs (or the empty pCambia 1391Z vector as negative controls) were subjected to histochemical staining.

GUS expression in transgenic *A. annua* plants

GUS staining was performed by incubating leaves and stems in staining solution (0.1 M sodium phosphate buffer [pH 7.0], 10 mM EDTA, 0.5 mM potassium ferrocyanide, 0.5 mM potassium ferricyanide, 1 mg/mL X-Gluc) at 37 °C in darkness for 12 h. Chlorophyll was removed by replacing the staining solution with 70% ethanol, followed by repeated ethanol washes until complete tissue decolorization.

Measurement of artemisinin content

A. annua leaves were collected for the test. Leaf samples were dried at 50 °C for 48 h and then ground into powder. The leaf powder was extracted twice with 2 ml of methanol using ultrasonication, with each sonication step lasting 30 min[45]. After extraction, the supernatant was centrifuged for 5 min and filtered through a 0.22 μm nitrocellulose membrane filter. Artemisinin content was measured using High Performance Liquid Chromatography (HPLC), following procedures described in previous literature[44].

RNA extraction and qRT-PCR analysis

Total RNA was extracted using the RNAprep Pure Plant Kit (Tiangen, Beijing, China) following the manufacturer's instructions. cDNA was synthesized using PrimeScript™ RT Master Mix (Takara, Shiga, Japan). Quantitative RT-PCR analysis was performed following procedures described in previous literature. The transcription levels of the genes were normalized using the *A. annua Actin* gene as an internal reference. All primers used are listed in Supplementary Table S3.

Yeast one hybrid assays

The full-length coding sequences of *AaHD8* were amplified using primers listed in Supplementary Table S3 and cloned into the pB42AD vector. Two concatenated L1-box-like motifs from the *AaLTP1* and *AaLTP2* promoters were inserted into pLacZ. The effector and reporter plasmids were co-transformed into the yeast strain EGY48a. The empty pB42AD vector was used as a control. Transformed yeast cells were cultured on SD/-Trp/-Ura medium. Positive clones were transferred to SD/-Trp/-Ura medium containing X-β-gal and cultured until a blue reaction appeared. All primers used for amplifying promoters and DNA motifs are listed in Supplementary Table S3.

Electrophoretic mobility shift assays

The full-length coding sequence of *AaHD8* was cloned into the pCold-TF vector (Takara) to generate a fusion protein with a His tag for protein expression and purification purposes. The pCold-AaHD8 construct was transformed into *Escherichia coli* Rosetta (DE3) strain (TransGen Biotech, China). An empty pCold-TF vector was also introduced into *Escherichia coli* Rosetta (DE3) as a negative control. Protein expression was induced by adding 0.5 mM isopropyl β-D-1-thiogalactopyranoside (IPTG) to the culture medium, and the induction was carried out at 16 °C for 14 h. The fusion protein was purified using Ni-NTA (Nickel-nitrilotriacetic acid) agarose (Invitrogen, USA) according to the manufacturer's instructions.

Electrophoretic Mobility Shift Assay (EMSA) was performed using biotin-labeled DNA probes as previously described and following the manufacturer's instructions[35]. Each reaction included 10 μg of recombinant His-TF and His-HD8. DNA probes AaLTP1-L1 and AaLTP2-L1 from the *AaLTP1* and *AaLTP2* promoters were synthesized by Sangon (Shanghai, China). Primers and probes used in the EMSA are listed in Supplementary Table S3.

Results

Identification, classification, and characteristics of *nsLTP* genes in *A. annua* L.

To identify the complete set of potential *nsLTP* genes in *A. annua*, a Hidden Markov Model (HMM) based on the *nsLTP* domain (PF00234) was utilized to search the *A. annua* proteome using HMMER-3.2.1 software. Initially, 116 proteins were retrieved. These sequences were then screened using SignalP to predict N-terminal signal peptide sequences (NSS), leading to the exclusion of six proteins lacking NSS. As mature *nsLTP* proteins typically have low molecular weights, 34 predicted mature proteins with more than 120 amino acids were further removed. Additionally, two proteins lacking the characteristic cysteine residue pattern were discarded. Proteins were then analyzed with the Web CD-Search tool to confirm the conserved domain, excluding 11 proteins lacking the LTP or AAI_LTSS structure. Finally, eight highly redundant sequences were removed through alignment and manual inspection, resulting in a total of 55 confirmed *nsLTP* genes in *A. annua* (Table 1).

These 55 AaLTPs were classified into eight types (I, II, III, IV, V, VI, VII, and IX) following the criteria established by Boutrot et al. (Table 1)[46], which is completely based on protein sequence similarity. This classification was manually curated without the use of automated tools. Given that LTPs are small proteins with conserved features, the established criteria were largely applicable to *A. annua*. A minor adjustment was made for *A. annua*-specific sequences: individuals with 17 or 20 amino acid residues between the fourth and fifth conserved cysteine residues were also categorized as type I, based on their high sequence similarity and phylogenetic analysis. The detailed classification basis is listed in Supplementary Table S4. All AaLTPs possess a signal peptide of 19–30 amino acids. It was found through the calculation tool DeepLoc-1.0 that, with the exception of *AaLTPVII.3*, which is predicted to localize to the cell membrane, the others are expected to be secreted into the extracellular space (Supplementary Table S5). The predicted molecular weights of the mature proteins range from 6,821 to 13,023 Da. Theoretical isoelectric point (pI) calculations show that 39 proteins have basic pI values (7.69–10.4), while the remaining proteins have acidic pI values (3.72–6.71). Predicted 3D structures are visualized in Supplementary Fig. S1. The ECM in all AaLTPs is highly conserved, forming four disulfide bonds that stabilize the hydrophobic cavity, similar to findings in rice, wheat, rape, and *Arabidopsis*[46,47]. Multiple sequence alignment of mature AaLTPs using ClustalX and visualizing with Jalview software (Fig. 1) demonstrated highly conserved eight cysteine residues and highlighted the diversity of the ECM domain and adjacent amino acid residues in *A. annua* (Table 2).

Phylogenetic analysis of the *nsLTP* family

To analyze the phylogenetic relationships within the *AaLTP* family, all 55 AaLTP protein sequences were used to construct an unrooted phylogenetic tree using the Maximum likelihood method. This phylogenetic tree, visualized alongside motif analysis, domain

analysis, and gene structure analysis (Fig. 2), revealed the evolutionary relationships among the nsLTPs in *A. annua*. All of the nsLTPs clustered according to their types, forming distinct branches on the evolutionary tree. Motif analysis indicated that nsLTPs of the same type typically contain similar motifs in type and number. Gene structure analysis results were visible for all genes except *AaLTPI.1* (*mRNA: Super-Scaffold_100123g01462191*), *AaLTPI.18* (*mRNA: unctg_3864g01516351*), and *AaLTPIII.1* (*mRNA: unctg_5142g01560471*), which lacked gene annotation files (see domain analysis results for these genes in Supplementary Fig. S2).

Table 1. Putative *nsLTP* genes identified in the genome of *A. annua* L.

	Name	Gene ID	CDS length (bp)	AA[a]	SP[b]	SL[c]	MP[d] (AA)	ECM[e]	MP (MW[f])	MP (pI[g])
Type I	*AaLtpI.1*	Super-scaffold_100123g01462191	351	116	25	s	91	C-X9-C-X13-CC-X19-CXC-X22-C-X13-C	9,106.48	9
	AaLtpI.2	chr2g00359671	345	114	25	s	89	C-X9-C-X13-CC-X17-CXC-X22-C-X13-C	9,016.44	8.87
	AaLtpI.3	chr2g00359701	333	110	25	s	85	C-X9-C-X13-CC-X17-CXC-X22-C-X13-C	8,599.97	8.7
	AaLtpI.4	chr3g00499441	345	114	25	s	89	C-X9-C-X13-CC-X19-CXC-X21-C-X12-C	9,076.39	9.05
	AaLtpI.5	chr1g00152381	411	136	24	s	112	C-X9-C-X13-CC-X19-CXC-X21-C-X13-C	12,177.13	5.54
	AaLtpI.6	chr2g00297041	351	116	25	s	91	C-X9-C-X13-CC-X19-CXC-X22-C-X13-C	9,439.93	9.19
	AaLtpI.7	chr2g00297131	351	116	25	s	91	C-X9-C-X13-CC-X19-CXC-X22-C-X13-C	9,198.68	9.57
	AaLtpI.8	chr2g00297171	348	115	25	s	90	C-X9-C-X13-CC-X19-CXC-X21-C-X13-C	9,019.42	9.26
	AaLtpI.9	chr2g00297151	351	116	25	s	91	C-X9-C-X13-CC-X19-CXC-X22-C-X13-C	9,092.46	9.3
	AaLtpI.10	chr2g00297111	354	117	25	s	92	C-X9-C-X13-CC-X19-CXC-X22-C-X13-C	9,763.21	8.66
	AaLtpI.11	chr3g00546061	369	122	29	s	93	C-X9-C-X16-CC-X19-CXC-X21-C-X13-C	9,745.02	3.72
	AaLtpI.12	chr2g00297121	342	113	19	s	94	C-X9-C-X13-CC-X19-CXC-X22-C-X13-C	10,230.87	8.67
	AaLtpI.13	chr1g00017271	360	119	27	s	92	C-X9-C-X14-CC-X19-CXC-X21-C-X13-C	9,043.43	8.89
	AaLtpI.14	chr2g00309551	354	117	24	s	93	C-X9-C-X14-CC-X19-CXC-X22-C-X13-C	9,682.74	4.14
	AaLtpI.15	chr4g00612411	369	122	29	s	93	C-X9-C-X14-CC-X19-CXC-X22-C-X13-C	10,033.22	4.76
	AaLtpI.16	chr6g01084791	363	120	28	s	92	C-X9-C-X14-CC-X20-CXC-X21-C-X13-C	9,795.49	7.69
	AaLtpI.17	chr2g00297031	360	119	22	s	97	C-X9-C-X15-CC-X19-CXC-X22-C-X12-C	10,454.11	9.3
	AaLtpI.18	unctg_3864g01516351	390	129	24	s	105	C-X9-C-X16-CC-X19-CXC-X23-C-X12-C	11,775.69	8.46
	AaLtpI.19	chr2g00297011	414	137	25	s	112	C-X9-C-X14-CC-X19-CXC-X22-C-X12-C	11,964.69	9.09
	AaLtpI.20	chr3g00499431	348	115	25	s	90	C-X9-C-X13-CC-X19-CXC-X21-C-X13-C	9,170.5	9.16
	AaLtpI.21	chr2g00297081	393	130	25	s	105	C-X9-C-X13-CC-X19-CXC-X22-C-X13-C	11,565.33	8.65
Type II	*AaLtpII.1*	chr1g00100031	294	97	27	s	70	C-X7-C-X13-CC-X8-CXC-X19-C-X3-C	7,771.9	8.47
	AaLtpII.2	chr1g00099971	297	98	25	s	73	C-X7-C-X13-CC-X8-CXC-X20-C-X2-C	7,861.2	5.06
	AaLtpII.3	chr1g00099961	285	94	26	s	68	C-X7-C-X13-CC-X8-CXC-X23-C-X6-C	7,196.39	8.88
	AaLtpII.4	chr5g00892001	288	95	27	s	68	C-X7-C-X13-CC-X8-CXC-X23-C-X6-C	7,424.05	9.96
	AaLtpII.5	chr1g00099991	294	97	27	s	70	C-X7-C-X13-CC-X8-CXC-X23-C-X6-C	7,999.08	8.95
	AaLtpII.6	chr3g00577871	291	96	25	s	71	C-X7-C-X13-CC-X8-CXC-X23-C-X6-C	7,771.01	8.5
	AaLtpII.7	chr6g01008841	363	120	25	s	95	C-X7-C-X16-CC-X9-CXC-X23-C-X9-C	10,504.09	4.75
	AaLtpII.8	chr3g00577891	294	97	29	s	68	C-X7-C-X13-CC-X8-CXC-X23-C-X6-C	7,165.38	8.91
	AaLtpII.9	chr9g01375721	294	97	28	s	69	C-X7-C-X13-CC-X8-CXC-X23-C-X6-C	7,633.87	8.89
	AaLtpII.10	chr5g00891931	294	97	29	s	68	C-X7-C-X13-CC-X8-CXC-X23-C-X6-C	7,245.69	9.41
	AaLtpII.11	chr3g00483861	300	99	30	s	69	C-X7-C-X14-CC-X8-CXC-X23-C-X6-C	7,522.63	7.74
Type III	*AaLtpIII.1*	unctg_5142g01560471	276	91	27	s	64	C-X9-C-X16-CC-X9-CXC-X12-C-X5-C	6,821.95	5.43
	AaLtpIII.2	chr3g00559411	282	93	27	s	66	C-X9-C-X17-CC-X9-CXC-X12-C-X5-C	7,061.03	5.43
Type IV	*AaLtpIV.1*	chr2g00348561	321	106	27	s	79	C-X9-C-X17-CC-X9-CXC-X17-C-X6-C	8,505.87	6.7
	AaLtpIV.2	chr8g01299581	294	97	22	s	75	C-X9-C-X15-CC-X9-CXC-X24-C-X6-C	7,822.12	4.34
Type V	*AaLtpV.1*	chr1g00206751	363	120	29	s	91	C-X14-C-X14-CC-X11-CXC-X16-C-X7-C	9,915.79	9.57
	AaLtpV.2	chr1g00206761	378	125	28	s	97	C-X14-C-X14-CC-X11-CXC-X24-C-X10-C	10,313.99	8.62
	AaLtpV.3	chr3g00569011	357	118	27	s	91	C-X14-C-X14-CC-X11-CXC-X24-C-X10-C	9,379.82	8.18
	AaLtpV.4	chr5g00787181	363	120	28	s	92	C-X14-C-X14-CC-X12-CXC-X24-C-X10-C	9,418.59	10.4
Type VI	*AaLtpVI.1*	chr6g01040821	318	105	22	s	83	C-X10-C-X12-CC-X9-CXC-X22-C-X9-C	9,389.32	10.33
	AaLtpVI.2	chr6g01040781	318	105	22	s	83	C-X10-C-X12-CC-X9-CXC-X22-C-X9-C	9,111.7	9.45
	AaLtpVI.3	chr1g00008331	336	111	29	s	82	C-X10-C-X16-CC-X9-CXC-X22-C-X9-C	8,667.06	6.71
	AaLtpVI.4	chr6g01040811	333	110	25	s	85	C-X10-C-X12-CC-X9-CXC-X23-C-X9-C	9,188.67	8.53
Type VII	*AaLtpVII.1*	chr1g00063881	333	110	27	s	83	C-X9-C-X14-CC-X12-CXC-X18-C-X7-C	8,888.1	4.39
	AaLtpVII.2	chr1g00063861	330	109	27	s	82	C-X9-C-X14-CC-X12-CXC-X18-C-X7-C	8,722.86	4.25
	AaLtpVII.3	chr2g00408761	423	140	26	s	114	C-X9-C-X14-CC-X12-CXC-X25-C-X9-C	12,044.73	4.51
	AaLtpVII.4	chr2g00415681	345	114	23	s	91	C-X9-C-X14-CC-X12-CXC-X26-C-X9-C	9,136.58	8.45
Type IX	*AaLtpIX.1*	chr2g00241771	339	112	24	s	88	C-X13-C-X15-CC-X9-CXC-X22-C-X6-C	9,369.99	8.21
nsLTPy	*nsLTPy.1*	chr4g00736531	270	89	26	s	63	C-X8-C-X13-CC-X8-CXC-X17-C-X6-C	6,862.86	4.59
	nsLTPy.2	chr4g00736521	273	90	27	s	63	C-X8-C-X13-CC-X8-CXC-X17-C-X6-C	6,910.89	4.56
	nsLTPy.3	chr2g00265921	399	132	26	s	106	C-X9-C-X12-CC-X19-CXC-X19-C-X14-C	12,314.22	8.44
	nsLTPy.4	chr2g00265911	405	134	25	s	109	C-X10-C-X13-CC-X19-CXC-X21-C-X14-C	12,409.34	8.98
	nsLTPy.5	chr4g00694091	423	140	26	s	114	C-X9-C-X22-CC-X19-CXC-X25-C-X14-C	12,533.12	9.44
	nsLTPy.6	chr2g00265901	423	140	25	s	115	C-X9-C-X12-CC-X19-CXC-X21-C-X14-C	13,023.16	8.44

[a] AA, number of amino acids; [b] SP, signal peptide; [c] SL, subcellular location, s = secretory pathway; [d] MP, mature protein; [e] ECM, eight cysteine motif; [f] MW, molecular weight in Dalton; [g] pI, isoelectric point. The detailed classification basis is listed in Supplementary Table S4.

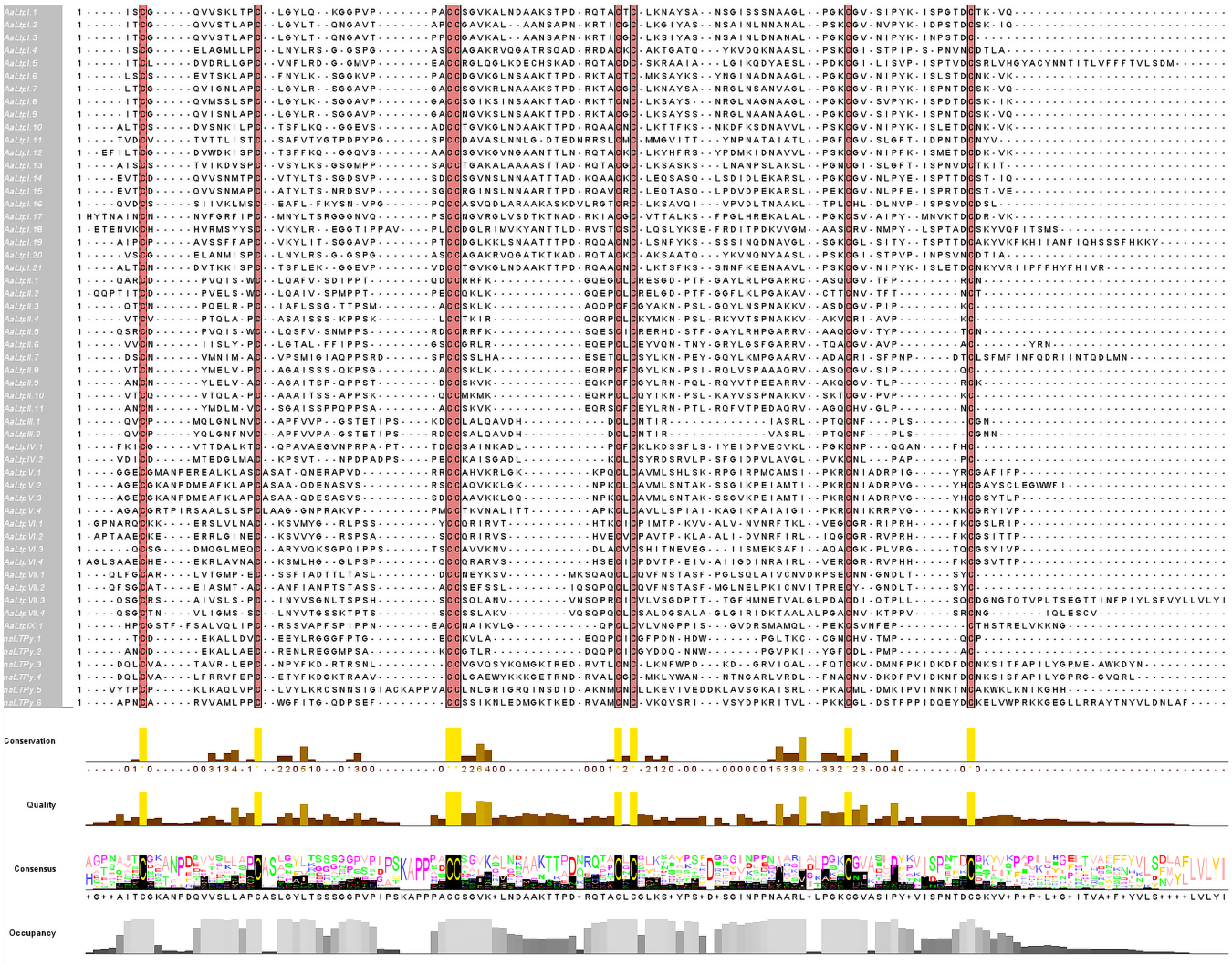

Fig. 1 Alignment of multiple sequences of AaLTP proteins. The conserved cysteine residues are marked against red backgrounds.

Table 2. Diversity of the eight cysteine motif.

nsLTP type	ECM and number of flanking amino acid residues														
		1		2		3, 4		5		6		7		8	
Type I	X	C	X9	C	X13–16	CC	X17, 19, 20	C	X	C	X21–23	C	X12, 13	C	X
Type II	X	C	X7	C	X13, 14, 16	CC	X8, 9	C	X	C	X19, 20, 23	C	X2, 3, 6, 9	C	X
Type III	X	C	X9	C	X16, 17	CC	X9	C	X	C	X12	C	X5	C	X
Type IV	X	C	X9	C	X15, 17	CC	X9	C	X	C	X17, 24	C	X6	C	X
Type V	X	C	X14	C	X14	CC	X11, 12	C	X	C	X16, 24	C	X7, 10	C	X
Type VI	X	C	X10	C	X12, 16	CC	X9	C	X	C	X22, 23	C	X9	C	X
Type VII	X	C	X9	C	X14	CC	X12	C	X	C	X18, 25, 26	C	X7, 9	C	X
Type IX	X	C	X13	C	X15	CC	X9	C	X	C	X22	C	X6	C	X
Type XI	X	C	X9	C	X18–20	CC	X13	C	X	C	X24, 25	C	X9	C	X

To further investigate the evolutionary relationship of the *nsLTP* families between *A. thaliana* and *A. annua*, a phylogenetic tree was constructed using the Maximum likelihood method with their 46 and 55 protein sequences, respectively (Fig. 3). The results showed that all nsLTPs could be classified into six clusters (A to F). Type I LTPs were all grouped within cluster A. Type II LTPs were grouped in cluster C, with the exception of one gene (*AaLTP II.7*). Type III and Type IX LTPs were grouped in cluster E, while cluster D consisted entirely of Type V and Type VII LTPs. Interestingly, *AaLTP VI* and *AtLTP VI* were grouped in cluster F and cluster B, respectively, with the exception of *AaLTP VI.3* in cluster B. Meanwhile, *AtLTP IV.3-5* and *AtLTP VI* were clustered together in cluster B, whereas an orthologous relationship was observed between *AtLTP IV.1/IV.2* and *AaLTP IV.1/IV.2*, which clustered together in cluster E. Three *A. thaliana* genes (*At3g12545-AtLTPII.8*, *At3g29105-AtLTPII.10*, and *At3g52310-AtLTPIX.2*) were excluded from the analysis because their predicted mature proteins lacked the conserved ECM structure, which could have potentially interfered with the multiple sequence alignment.

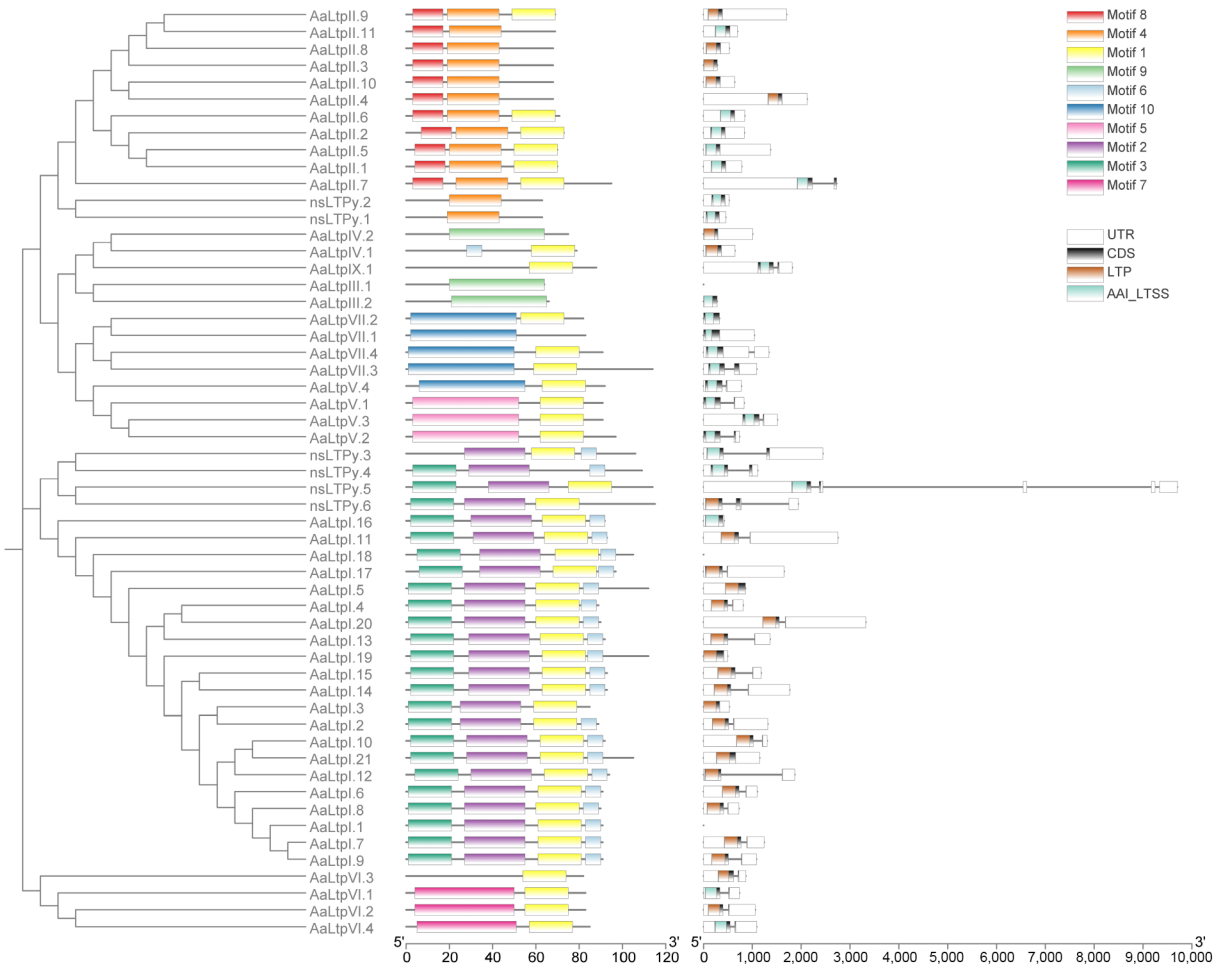

Fig. 2 Phylogenetic tree of AaLTPs together with motif analysis and gene structure analysis. The full length of mature protein sequences of nsLTPs from *A. annua* was used to construct the phylogenetic tree using a Maximum likelihood method. Motif analysis was performed using MEME, while domain analysis was performed using the batch Web CD-Search tool. All of the above results were visualized together with the gene annotation file.

Expression analysis of *nsLTP* genes

Analysis of RNA-seq data from six different kinds of organs (roots, stems, leaves, seeds, buds, and trichomes) was used to determine the expression patterns of *AaLTP* genes[42]. Genes with an RPKM value ≥ 1 were considered positively expressed. As a result, 39 (71%) *AaLTP* genes were found to be expressed in at least one organ (Fig. 4; Supplementary Table S6). Some genes exhibited specific expression patterns in different organs. For example, *chr2g00297041-AaLTPI.6*, *chr2g00309551-AaLTPI.14*, *chr4g00612411-AaLTPI.15*, and *chr1g00206751-AaLTPV.1* were specifically expressed in trichomes. *chr3g00577891-AaLTPII.8* and *chr5g00891931-AaLTPII.10* showed specific expression in leaves, while *chr1g00152381-AaLTPI.5* and *chr3g00499431-AaLTPI.20* exhibited specific expression in the seeds.

Since AaHD8, an HD-Zip IV transcription factor in *A. annua*, regulates the development of trichome and leaf cuticle, and the *LTP* gene is mostly related to cuticle, a potential relationship between *AaHD8* and *AaLTP* genes was investigated. Based on RNA-seq data from *AaHD8*-RNAi lines[43], four *AaLTP* genes showed significant expression differences (adjusted *p*-value < 0.05) between 0.038 and 9.19 FC (fold change) (Fig. 5). Specifically, two type I genes, *chr2g00297131-AaLTPI.7* and *chr2g00297171-AaLTPI.8*, exhibited significant upregulation, while two type I genes, *chr2g00309551-AaLTPI.14* and *chr2g00297041-AaLTPI.6*, showed significant downregulation.Expressionof*chr2g00309551-AaLTPI.14*and*chr2g00297041-AaLTPI.6* decreased significantly by 114-fold and 86-fold, respectively, compared to the wild-type (WT), indicating direct regulation of these *AaLTP* genes by *AaHD8*, which activated their expression (Supplementary Fig. S3). These findings suggest a regulatory role of *AaHD8* in the expression of these *AaLTP* genes.

Cloning and expression pattern analysis of *AaLTP1* and *AaLTP2*

AaLTPI.14 and *AaLTPI.6* exhibited specific and high expression in glandular trichomes (Fig. 4) and were significantly down-regulated in *AaHD8*-RNAi plants (Fig. 5). Based on their predominant expression and importance, these two genes were cloned and named *AaLTP1* and *AaLTP2*, respectively, following the nomenclature convention for key nsLTPs established in model plants like *O. sativa* and *A. thaliana*. To investigate their spatial expression patterns, promoter regions—1,967 bp for *AaLTP1* and 1,171 bp for *AaLTP2*—were cloned into the 1391Z-proAaLTP1-GUS and 1391Z-proAaLTP2-GUS vectors, respectively, and these constructs were transformed into *A. annua* plants. GUS staining of transgenic plants revealed that both genes are specifically expressed in young leaves, particularly in GSTs, as opposed to T-shaped non-GSTs (TSTs) (Fig. 6). This expression pattern aligns with the RNA-seq data previously determined

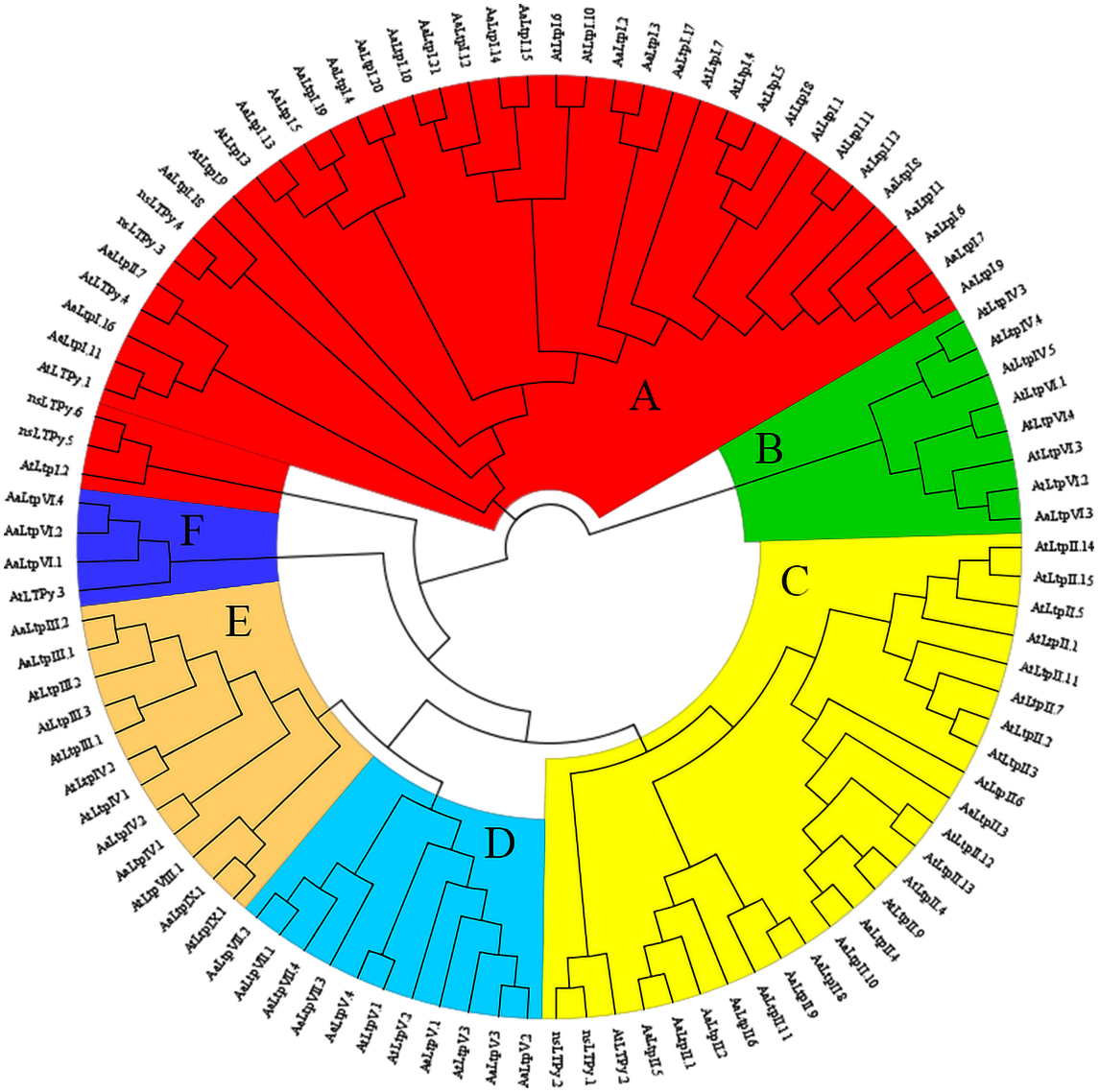

Fig. 3 Phylogenetic tree of nsLTPs in *A. thaliana* and *A. annua*. The full length of mature protein sequences of nsLTPs from *A. thaliana* and *A. annua* were used to construct the phylogenetic tree using a Maximum likelihood method. Different colors represent different clusters.

(Fig. 4), confirming the specificity of *AaLTP1* and *AaLTP2* expression in glandular trichomes.

Enhanced production of artemisinin in transgenic *AaLTP1*-OE plants

Given that *AaLTP1* exhibited the most significant downregulation in *AaHD8*-RNAi plants, to further explore the function of the *AaLTP1* gene, transgenic plants overexpressing *AaLTP1* (*AaLTP1*-OE) were generated. Positive transgenic plants were confirmed by PCR, and the expression levels of *AaLTP* transcripts were validated by qRT-PCR. Subsequently, three independent transgenic lines showing a two to three-fold increase in *AaLTP1* mRNA level were selected for further analysis (Fig. 7).

The artemisinin content in the *AaLTP1*-OE plants was analyzed using High Performance Liquid Chromatography (HPLC). The results demonstrated that the artemisinin content in *AaLTP1*-OE plants increased by 1.6 times compared to the WT (Fig. 8), indicating that over-expression of the *AaLTP1* gene promotes artemisinin accumulation in *A. annua*.

AaHD8 positively regulates *AaLTP* gene expression through direct binding to the promoter

AaHD8, a member of the HD-Zip IV gene family, was hypothesized to bind to the L1-box cis-element (5'-TAAATG(C/T) A-3') due to its known affinity for this sequence[48]. Analysis of the *AaLTP* gene promoters using PlantPAN 3.0 identified L1-box-like sequences, suggesting that *AaHD8* may interact with these regions. This hypothesis was tested through yeast one-hybrid assays, which confirmed that *AaHD8* binds to the L1-box-like sequences in the promoters of *AaLTP1* and *AaLTP2* (Fig. 9). Electrophoretic mobility shift assays (EMSA) using recombinant His-tagged AaHD8 and His-tagged trigger factor (TF) purified from *Escherichia coli* further validated this interaction. A distinct shifted band was observed with His-AaHD8 and a biotin-labeled L1 probe, with no binding seen with His-TF or a mutated probe (Fig. 9). These results demonstrate that *AaHD8* regulates the expression of *AaLTP1* and *AaLTP2* by directly binding to the L1-box-like motifs in their promoters.

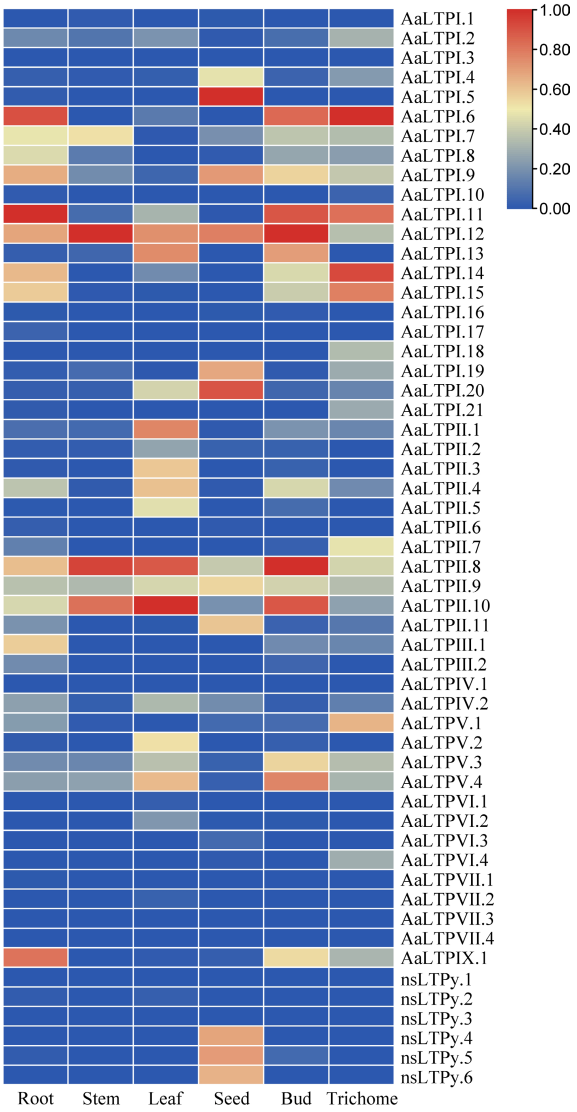

Fig. 4 Expression analysis of *AaLTPs*. The heatmap shows expression comparison between six organs of *AaLTPs*. The data shown were the results of column scaling each gene by RNA-seq data using the Zero To One Scale Method. The color bar represents the relative expression level.

To validate the regulatory role of *AaHD8* on *AaLTP* expression in vivo, qRT-PCR analysis was performed using WT *A. annua* and transgenic plants overexpressing *AaHD8* (Fig. 10). Compared to WT, *AaHD8* overexpression increased the expression of *AaLTP1* and *AaLTP2* genes by 2.2 to 4.9 times and 2.3 to 4.5 times, respectively, in five independent *AaHD8* overexpressing plants. These results indicated that *AaHD8* overexpression can directly activate the expression of *AaLTP1* and *AaLTP2* in *A. annua* plants.

Discussion

This study presents the first comprehensive genome-wide analysis of nsLTPs in *A. annua* and their involvement in artemisinin biosynthesis. The identification of *AaLTP1* and *AaLTP2* as glandular trichome-specific nsLTPs highlights their potential role in facilitating the intracellular trafficking of metabolites in these specialized tissues. Indeed, the 1.5-fold increase in artemisinin content observed in *AaLTP1*-overexpressing lines provides strong evidence

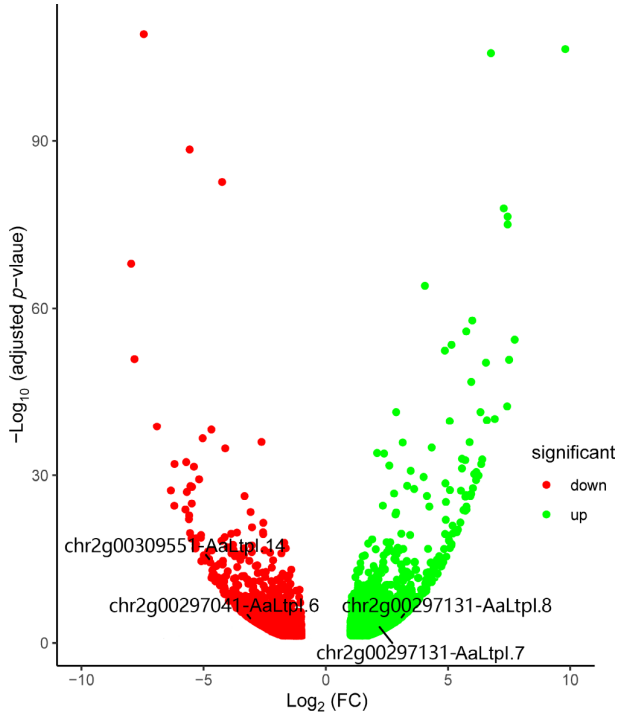

Fig. 5 Volcano plot shows differentially expressed genes in *AaHD8*-RNAi. The red points indicate down-regulated genes, while the green ones indicate up-regulated genes. FC stands for fold change.

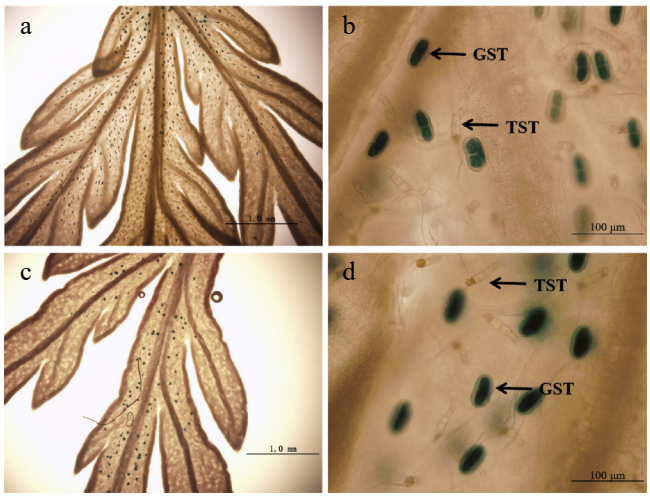

Fig. 6 GUS expression (blue) in *A. annua* plants transformed with the 1391Z-proLTP1-GUS and 1391Z-proLTP2-GUS vector. (a), (b) Leaves of 1391Z-proLTP1-GUS plants. (c), (d) Leaves of 1391Z-proLTP2-GUS plants.

that these proteins directly contribute to artemisinin production. This finding contrasts with earlier reports where *AaLTP1* and *AaLTP2* showed minimal effects on dihydroartemisinic acid (DHAA) accumulation[49], suggesting functional divergence or context-dependent regulation within the *nsLTP* family. While prior studies implicated *AaLTP3* and *AaLTP4* in sesquiterpene secretion[31], results establish *AaLTP1* as a key regulator of artemisinin biosynthesis, underscoring the need to dissect isoform-specific roles in lipid trafficking.

Comprehensive analysis of the *nsLTP* gene family in *A. annua* reveals a significant number of 55 *nsLTP* genes, encompassing diverse types, including 21 type I, 11 type II, two type III, two type IV, four type V, four type VI, four type VII, one type IX, and six *nsLTPy*

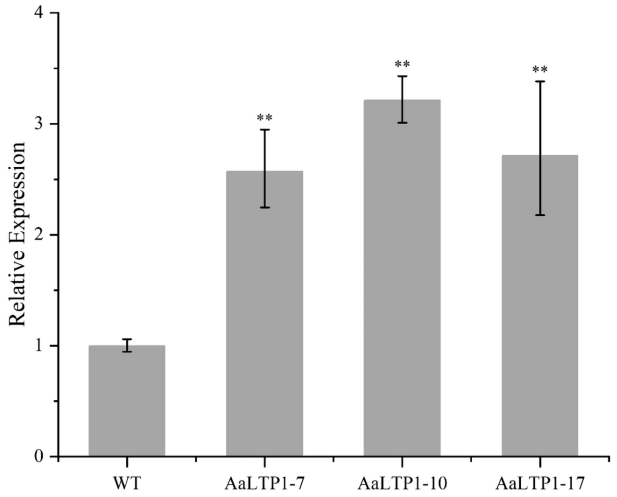

Fig. 7 Expression levels of *AaLTP1* in *AaLTP1* over-expression plants measured by qRT-PCR. The average expression level of genes in WT was set as 1. *Actin* was used as internal control; the error bars show means ± SD from three technical repeats; Student's *t*-test ** $p < 0.01$, * $p < 0.05$.

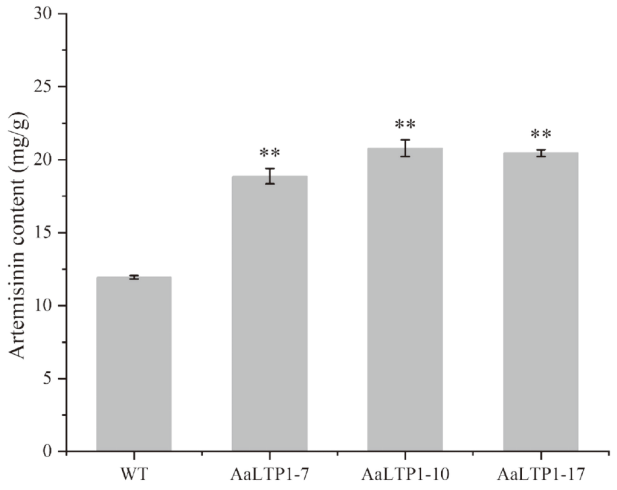

Fig. 8 Artemisinin contents in *AaLTP1* over-expression lines were measured by HPLC. Error bars indicate ± SD of three biological replicates. ** $p < 0.01$, Student's *t*-test.

(Table 1). This study provides a detailed characterization of these genes, in contrast to other plant species such as *Arabidopsis*, rice, rape, and maize, which have been reported to contain 49, 52, 63, and 63 nsLTPs, respectively. Notably, *A. annua* lacks *nsLTP* types VIII, X, and XI (Table 2), a loss that is consistent with the absence of type XI nsLTPs in monocotyledonous plants and suggests an evolutionary divergence between monocots and dicots. Despite the identification of proteins resembling type XI nsLTPs in *A. annua*, domain analysis confirmed that these do not possess the requisite LTP or AAI_LTSS structures, thus excluding them from classification as nsLTPs.

The glandular trichome-specific expression of *AaLTP1* and *AaLTP2* strongly implies their involvement in the transport of hydrophobic precursors essential for artemisinin biosynthesis. A key question is how extracellularly localized nsLTPs might access cytosolic substrates like FPP or potentially organellar DHAA. It is hypothesized that this may involve an intermediate step: these precursors are first actively transported across the plasma membrane or organellar membranes by specific transporters, thereby becoming accessible to the apoplastic nsLTPs. *AaLTP1* and *AaLTP2* could then function as extracellular shuttles, facilitating the subsequent movement of these precursors through the glandular trichome secretory space or towards the site of final artemisinin assembly and storage. Structural studies across plant species provide mechanistic clues: nsLTPs universally feature a hydrophobic cavity stabilized by disulfide bonds[50,51], enabling lipid binding. For instance, in *Solanum melongena*, *nsLTP* binds lipids through a dynamic process where surface-bound intermediates transiently interact before internalization into the cavity, mediated by conformational changes in 'gating' residues[52]. Similarly, the crystal structure of wheat *nsLTP* revealed dual lipid binding—one in the main cavity and another in an adjacent pocket[50]—suggesting a capacity for simultaneous transport of distinct lipophilic molecules. In *A. annua*, *AaLTP1* and *AaLTP2* may utilize this conserved mechanism to sequester artemisinin precursors such as dihydroartemisinic acid (DHAA) or farnesyl pyrophosphate (FPP) within their hydrophobic cavities, shielding these intermediates from degradation while facilitating their movement across cellular compartments and surrounding tissues, including vascular systems, which may be critical for the efficient delivery of precursors to the artemisinin biosynthetic pathway[53–55]. The observed 1.5-fold increase in artemisinin content in *AaLTP1*-OE lines supports this hypothesis. Structural analysis of *Kalanchoe fedtschenkoi nsLTP*[56] demonstrated direct binding of lauric acid within the hydrophobic cavity, a feature likely conserved in AaLTPs. Additionally, the hydrogen bond-mediated closure of the binding pocket observed in eggplant *nsLTP*[51] suggests that environmental cues (e.g., pH shifts in glandular trichomes) or interactions with partner proteins could regulate lipid release from AaLTPs, thereby synchronizing precursor availability with biosynthetic demands. To rigorously test these hypotheses and clarify the trafficking route, future studies must include molecular docking simulations to predict their affinity for artemisinin precursors like DHAA and FPP. Furthermore, *in vitro* lipid-binding assays using purified proteins and isotopic tracing of precursor trafficking in transgenic lines will be essential.

The localization of *AaLTP1* and *AaLTP2* in glandular trichomes aligns with the conserved role of nsLTPs in specialized metabolite transport across plant species, yet highlights species-specific adaptations for distinct secondary metabolites. In *Mentha canadensis*, nsLTPs such as *McLTPII.9* enhance peltate glandular trichome density and monoterpene biosynthesis[57], while in *Tanacetum parthenium*, trichome-specific *TpLTP1* and *TpLTP2* mediate extracellular accumulation of sesquiterpene lactones like costunolide and parthenolide[58]. Similarly, *AaLTP1* and *AaLTP2* likely evolved to facilitate artemisinin precursor transport in *A. annua* glandular trichomes. This role is not unique to *A. annua*: the involvement of nsLTPs in trafficking precursors or cofactors essential for secondary metabolite biosynthesis in glandular trichomes is well-documented in plants such as *Salvia fruticosa*[59], hop[60], *Cistus creticus*[61], *A. annua*[62], alfalfa[63], basil[64], and peppermint[65], where lipid transfer proteins mediate transport across membranes in specialized cells. However, substrate specificity varies significantly among species. For instance, *TpLTP3* in feverfew exhibits strict selectivity for parthenolide export[58], whereas *AaLTP1* may preferentially bind artemisinin precursors such as DHAA, analogous to the lauric acid-binding activity observed in *Kalanchoe fedtschenkoi nsLTP*[56]. This functional divergence underscores how nsLTPs are tailored to the unique metabolic demands of their host plants. Notably, nsLTPs in non-glandular tissues also play conserved roles in lipid barrier formation. For example, castor bean *nsLTP* regulates fatty acid β-oxidation in glyoxysomes[66], while Arabidopsis LTPs contribute to cuticular wax synthesis[67]. In contrast, *AaLTP1* and *AaLTP2* appear specialized for glandular trichome biology, mirroring the trichome-specific roles of *McLTPII.9*[57] and *TpLTP1/2*[58]. This tissue-specific specialization

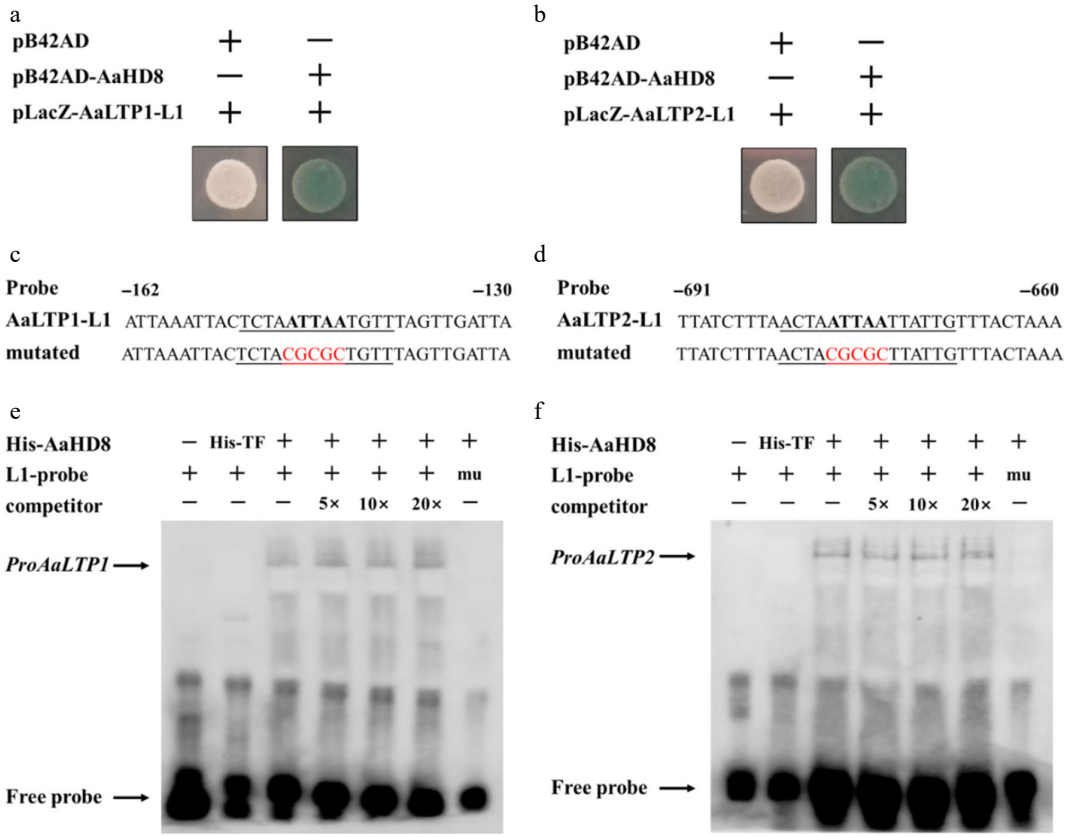

Fig. 9 *AaHD8* directly binds to the promoter of *AaLTP1* and *AaLTP2*. (a), (b) Yeast one-hybrid assay of protein–DNA interaction. pB42AD is an empty vector used as a negative control. (c), (d) Probe and mutant probe. (e), (f) *AaHD8* binds to the L1-box-like motif from *AaLTP*; 5×, 10×, and 20× indicate the dilution multiple of cold competitors relative to that of the labeled probe; mu: labeled mutated L1-probes were tested as negative controls; His-TF protein was used as a negative control.

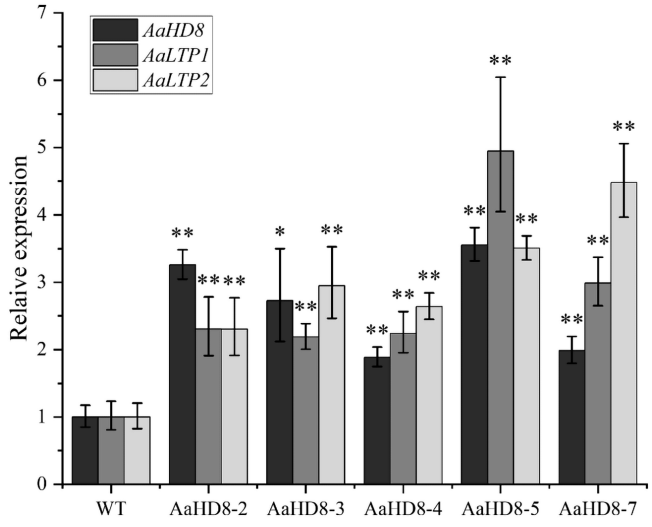

Fig. 10 Relative expression of *AaHD8* and *AaLTP* in *AaHD8* overexpression plants. The average expression level of genes in WT was set as 1. *Actin* was used as internal control; the error bars show means ± SD from three technical repeats; Student's *t*-test ** $p < 0.01$, * $p < 0.05$.

suggests that while nsLTPs broadly mediate lipid trafficking, their recruitment to glandular trichomes represents an evolutionary adaptation to enhance the production and secretion of high-value metabolites like artemisinin.

The identification of AaHD8, an HD-ZIP IV transcription factor involved in cuticle biosynthesis and trichome initiation[43], as a direct regulator of *AaLTP1* and *AaLTP2* expands understanding of *nsLTP* regulation in *A. annua*. HD-ZIP transcription factors are known integrators of developmental and environmental signals—such as light, temperature, and biotic stress—that modulate secondary metabolism[68,69]. Findings suggest that *AaHD8* may orchestrate artemisinin biosynthesis by linking lipid transport (*AaLTP1/2* expression) with trichome development and stress adaptation; for example, upregulation of *AaLTP1* and *AaLTP2* via *AaHD8* might be part of a broader adaptive mechanism to optimize artemisinin production under fluctuating environmental conditions. This regulatory nexus aligns with observations in other medicinal plants, where HD-ZIPs coordinate metabolite production and abiotic stress responses[70]. Future studies should investigate whether AaHD8 interacts with MYB or WRKY transcription factors to fine-tune *AaLTP* expression and explore its broader role in artemisinin pathway regulation via ChIP-seq or promoter mutagenesis.

The identification and functional characterization of *AaLTP1* and *AaLTP2* provide a potential route for biotechnological enhancement of artemisinin production. Overexpression of these genes in engineered *A. annua* could be an effective strategy for increasing the yield of artemisinin. Furthermore, the regulation of *AaLTP1* and *AaLTP2* by *AaHD8* suggests that manipulating this transcription factor could enhance artemisinin production under controlled environmental conditions. Understanding the environmental and genetic factors that influence AaHD8 activity could help in designing plants with enhanced resistance to abiotic stresses while simultaneously boosting the production of this important pharmaceutical compound.

While this study has provided valuable insights into the role of nsLTPs in *A. annua*, several questions remain unanswered. For instance, the precise mechanism by which *AaLTP1* and *AaLTP2* influence lipid and artemisinin metabolism at the molecular level is still unclear. Notably, RNA-seq data revealed additional *nsLTP* candidates potentially involved in glandular trichome biology: *AaLTPI.11* is highly expressed in both glandular trichomes and roots, suggesting dual roles in metabolite transport across tissues; *AaLTPI.15* and *AaLTPV.1*, though trichome-specific, exhibit lower expression levels compared to *AaLTP1/2*, implying subsidiary or stage-specific functions. Intriguingly, in *AaHD8*-RNAi plants, *AaLTPI.7* and *AaLTPI.8* were upregulated—contrary to the downregulation of *AaLTP1/2*—hinting at compensatory mechanisms or divergent regulatory networks among *nsLTP* isoforms. It is worth noting that the observed phenotypic changes are unlikely to be attributed to alterations in trichome development, as no significant differences in trichome density or morphology were detected, which reinforces the proposed direct role of *AaLTP1/2* in lipid transport. Future research should therefore focus on identifying the specific lipid ligands bound by these proteins, their interactions with artemisinin biosynthetic enzymes, and the regulatory logic underlying their opposing expression patterns. Additionally, exploring the roles of other trichome-enriched nsLTPs in stress responses could provide a holistic understanding of lipid metabolism in *A. annua*.

In summary, these findings represent an important step in elucidating the role of lipid transfer proteins in *A. annua* and their contribution to artemisinin biosynthesis. The functional validation of *AaLTP1* and *AaLTP2*, along with the identification of AaHD8 as a key regulator, opens new avenues for both basic and applied research. Future studies should focus on resolving the molecular mechanisms by which *AaLTP1* facilitates artemisinin precursor transport, including *in vitro* ligand-binding assays and spatial tracking of lipid trafficking within glandular trichomes. The broader regulatory network involving AaHD8 and its potential crosstalk with other trichome-specific transcription factors (e.g., MYB or WRKY families) warrants systematic exploration through chromatin immunoprecipitation and multi-omics approaches. By bridging mechanistic insights with metabolic engineering strategies, this work provides a new strategy for increasing the yield of artemisinin through genetic engineering methods while advancing understanding of *nsLTP* functionality in plant metabolism.

Conclusions

In this study, the first genome-wide identification and functional characterization of the *nsLTP* gene family in *A. annua*, a medicinal plant renowned for its production of the antimalarial compound artemisinin, was conducted. A total of 55 *nsLTP* genes were identified and classified into eight distinct types, revealing both conserved and species-specific features in their gene structure, motif composition, and evolutionary relationships. Notably, expression profiling and promoter-GUS assays demonstrated that *AaLTP1* and *AaLTP2* are specifically expressed in glandular secretory trichomes—the primary sites of artemisinin biosynthesis.

Functional analyses revealed that overexpression of *AaLTP1* significantly enhances artemisinin accumulation, underscoring its direct role in the artemisinin biosynthetic pathway. Furthermore, the HD-Zip IV transcription factor AaHD8 was established as a positive regulator of *AaLTP1* and *AaLTP2* by directly binding to L1-box-like motifs in their promoters. This regulatory link integrates trichome development with lipid transport mechanisms, highlighting a coordinated network that supports artemisinin production.

These findings not only expand the understanding of *nsLTP* functions in specialized metabolism but also provide a genetic toolkit for metabolic engineering aimed at increasing artemisinin yield. Future studies should focus on elucidating the specific lipid substrates of *AaLTP1/2*, their interaction with artemisinin biosynthetic enzymes, and the broader regulatory circuitry involving AaHD8 and other trichome-specific transcription factors. This work lays a foundation for leveraging lipid transfer proteins in biotechnological strategies to enhance the production of high-value plant metabolites.

Author contributions

The authors confirm their contributions to the paper as follows: study conception and design: Wen H, Wang W, Yan S, Li L; data collection: Wang W, Liu H, Wu E; analysis and interpretation of results: Wen H, Wang W, He W, Liu H, Su L, Hu X, Yan X; investigation: Wen H, Wang W, Liu H, Su L, Hu X, Yan X, Peng B, Zhang Y, Liu P; methodology: Wen H, Wang W; software: Wen H; visualization: Wen H; draft manuscript preparation: Wen H, Wang W; writing – review & editing: He W, Yan S, Li L; supervision: Tang K, Li L; project administration: Fu X, Ren L, Tang K, Li L; resources: Tang K; funding acquisition: Tang K, Li L. All authors reviewed the results and approved the final version of the manuscript.

Data availability

All data generated or analyzed during this study are included in this published article and its supplementary information files.

Acknowledgments

This work was supported by the National Natural Science Foundation of China (Grant Nos. 32070329, 31770327), the Natural Science Foundation of Shanghai (Grant No. 25ZR1401180), the National Key R&D Program of China (Grant No. 2018YFA0900600), and the Bill & Melinda Gates Foundation (Grant No. OPP1199872).

Conflict of interest

The authors declare that they have no conflict of interest.

Supplementary information accompanies this paper online at: https://doi.org/10.48130/mpb-0025-0040.

Dates

Received 10 August 2025; Revised 15 October 2025; Accepted 5 November 2025; Published online 19 January 2026

References

[1] Klayman DL. 1985. *Qinghaosu* (artemisinin): an antimalarial drug from China. *Science* 228:1049–1055

[2] Olsson ME, Olofsson LM, Lindahl AL, Lundgren A, Brodelius M, et al. 2009. Localization of enzymes of artemisinin biosynthesis to the apical cells of glandular secretory trichomes of *Artemisia annua* L. *Phytochemistry* 70:1123–1128

[3] Wang Z, Qiu J, Guo TB, Liu A, Wang Y, et al. 2007. Anti-inflammatory properties and regulatory mechanism of a novel derivative of artemisinin in experimental autoimmune encephalomyelitis. *The Journal of Immunology* 179:5958–5965

[4] Efferth T, Romero MR, Wolf DG, Stamminger T, Marin JJG, et al. 2008. The antiviral activities of artemisinin and artesunate. *Clinical Infectious Diseases* 47:804–811

[5] Crespo-Ortiz MP, Wei MQ. 2012. Antitumor activity of artemisinin and its derivatives: from a well-known antimalarial agent to a potential anticancer drug. *Journal of Biomedicine and Biotechnology* 2012:247597

[6] Kader JC, Julienne M, Vergnolle C. 1984. Purification and characterization of a spinach-leaf protein capable of transferring phospholipids from liposomes to mitochondria or chloroplasts. *European Journal of Biochemistry* 139:411–416

[7] Kader JC. 1996. Lipid-transfer proteins in plants. *Annual Review of Plant Physiology and Plant Molecular Biology* 47:627–654

[8] José-Estanyol M, Gomis-Rüth FX, Puigdomènech P. 2004. The eight-cysteine motif, a versatile structure in plant proteins. *Plant Physiology and Biochemistry* 42:355–365

[9] Douliez JP, Michon T, Elmorjani K, Marion D. 2000. Mini review: structure, biological and technological functions of lipid transfer proteins and indolines, the major lipid binding proteins from cereal kernels. *Journal of Cereal Science* 32:1–20

[10] DeBono A, Yeats TH, Rose JKC, Bird D, Jetter R, et al. 2009. *Arabidopsis* LTPG is a glycosylphosphatidylinositol-anchored lipid transfer protein required for export of lipids to the plant surface. *The Plant Cell* 21:1230–1238

[11] Maldonado AM, Doerner P, Dixon RA, Lamb CJ, Cameron RK. 2002. A putative lipid transfer protein involved in systemic resistance signalling in *Arabidopsis*. *Nature* 419:399–403

[12] Blein JP, Coutos-Thévenot P, Marion D, Ponchet M. 2002. From elicitins to lipid-transfer proteins: a new insight in cell signalling involved in plant defence mechanisms. *Trends in Plant Science* 7:293–296

[13] Cameron KD, Teece MA, Smart LB. 2006. Increased accumulation of cuticular wax and expression of lipid transfer protein in response to periodic drying events in leaves of tree tobacco. *Plant Physiology* 140:176–183

[14] Nieuwland J, Feron R, Huisman BAH, Fasolino A, Hilbers CW, et al. 2005. Lipid transfer proteins enhance cell wall extension in tobacco. *The Plant Cell* 17:2009–2019

[15] Park SY, Jauh GY, Mollet JC, Eckard KJ, Nothnagel EA, et al. 2000. A lipid transfer-like protein is necessary for lily pollen tube adhesion to an in vitro stylar matrix. *The Plant Cell* 12:151–163

[16] Zhang D, Liang W, Yin C, Zong J, Gu F, et al. 2010. *OsC6*, encoding a lipid transfer protein, is required for postmeiotic anther development in rice. *Plant Physiology* 154:149–162

[17] Chen C, Chen G, Hao X, Cao B, Chen Q et al. 2011. *CaMF2*, an anther-specific lipid transfer protein (LTP) gene, affects pollen development in *Capsicum annuum* L. *Plant Science* 181:439–448

[18] Coutos-Thevenot P, Jouenne T, Maes O, Guerbette F, Grosbois M, et al. 1993. Four 9-kDa proteins excreted by somatic embryos of grapevine are isoforms of lipid-transfer proteins. *European Journal of Biochemistry* 217:885–889

[19] Potocka I, Baldwin TC, Kurczynska EU. 2012. Distribution of lipid transfer protein 1 (LTP1) epitopes associated with morphogenic events during somatic embryogenesis of *Arabidopsis thaliana*. *Plant Cell Reports* 31:2031–2045

[20] Pagnussat L, Burbach C, Baluška F, de la Canal L. 2012. An extracellular lipid transfer protein is relocalized intracellularly during seed germination. *Journal of Experimental Botany* 63:6555–6563

[21] Sun JY, Gaudet DA, Lu ZX, Frick M, Puchalski B, et al. 2008. Characterization and antifungal properties of wheat nonspecific lipid transfer proteins. *Molecular Plant-microbe Interactions* 21:346–360

[22] Jia Z, Gou J, Sun Y, Yuan L, Tang Q, et al. 2010. Enhanced resistance to fungal pathogens in transgenic *Populus tomentosa* Carr. by overexpression of an nsLTP-like antimicrobial protein gene from motherwort (*Leonurus japonicus*). *Tree Physiology* 30:1599–1605

[23] Guo C, Ge X, Ma H. 2013. The rice *OsDIL* gene plays a role in drought tolerance at vegetative and reproductive stages. *Plant Molecular Biology* 82:239–253

[24] Guo L, Yang H, Zhang X, Yang S. 2013. *Lipid transfer protein 3* as a target of MYB96 mediates freezing and drought stress in *Arabidopsis*. *Journal of Experimental Botany* 64:1755–1767

[25] Wei K, Zhong X. 2014. Non-specific lipid transfer proteins in maize. *BMC Plant Biology* 14:281

[26] Edstam MM, Laurila M, Höglund A, Raman A, Dahlström KM, et al. 2014. Characterization of the GPI-anchored lipid transfer proteins in the moss *Physcomitrella patens*. *Plant Physiology and Biochemistry* 75:55–69

[27] Gonçalves GR, da Silva MS, dos Santos LA, Guimarães TZA, Taveira GB, et al. 2024. Structural and functional characterization of new lipid transfer proteins with chitin-binding properties: insights from protein structure prediction, molecular docking, and antifungal activity. *Biochemistry* 63:1824–1836

[28] Wang D, Song J, Lin T, Yin Y, Mu J, et al. 2023. Identification of potato Lipid transfer protein gene family and expression verification of drought genes *StLTP1* and *StLTP7*. *Plant Direct* 7:e491

[29] Maghraby A, Alzalaty M. 2024. Genome-wide identification and evolutionary analysis of the *AP2/EREBP*, *COX* and *LTP* genes in *Zea mays* L. under drought stress. *Scientific Reports* 14:7610

[30] Moraes GP, Benitez LC, do Amaral MN, Vighi IL, Auler PA, et al. 2015. Expression of LTP genes in response to saline stress in rice seedlings. *Genetics and Molecular Research* 14:8294–8305

[31] Adhikari PB, Han JY, Ahn CH, Choi YE. 2019. Lipid transfer proteins (AaLTP3 and AaLTP4) are involved in sesquiterpene lactone secretion from glandular trichomes in *Artemisia annua*. *Plant & Cell Physiology* 60:2826–2836

[32] Liao B, Shen X, Xiang L, Guo S, Chen S, et al. 2022. Allele-aware chromosome-level genome assembly of *Artemisia annua* reveals the correlation between *ADS* expansion and artemisinin yield. *Molecular Plant* 15:1310–1328

[33] Abe M, Katsumata H, Komeda Y, Takahashi T. 2003. Regulation of shoot epidermal cell differentiation by a pair of homeodomain proteins in *Arabidopsis*. *Development* 130:635–643

[34] Nadakuduti SS, Pollard M, Kosma DK, Allen C Jr, Ohlrogge JB, et al. 2012. Pleiotropic phenotypes of the *sticky peel* mutant provide new insight into the role of *CUTIN DEFICIENT2* in epidermal cell function in tomato. *Plant Physiology* 159:945–960

[35] Ma YN, Xu DB, Li L, Zhang F, Fu XQ, et al. 2018. Jasmonate promotes artemisinin biosynthesis by activating the TCP14-ORA complex in *Artemisia annua*. *Science Advances* 4:eaas9357

[36] He W, Liu H, Li Y, Wu Z, Xie Y, et al. 2023. Genome-wide characterization of B-box gene family in *Artemisia annua* L. and its potential role in the regulation of artemisinin biosynthesis. *Industrial Crops and Products* 199:116736

[37] He W, Liu H, Wu Z, Miao Q, Hu X, et al. 2024. The AaBBX21–AaHY5 module mediates light-regulated artemisinin biosynthesis in *Artemisia annua* L. *Journal of Integrative Plant Biology* 66:1735–1751

[38] Almagro Armenteros JJ, Sønderby CK, Sønderby SK, Nielsen H, Winther O. 2017. DeepLoc: prediction of protein subcellular localization using deep learning. *Bioinformatics* 33:3387–3395

[39] Kelley LA, Mezulis S, Yates CM, Wass MN, Sternberg MJE. 2015. The Phyre2 web portal for protein modeling, prediction and analysis. *Nature Protocols* 10:845–858

[40] Larkin MA, Blackshields G, Brown NP, Chenna R, McGettigan PA, et al. 2007. Clustal W and Clustal X version 2.0. *Bioinformatics* 23:2947–2948

[41] Kumar S, Stecher G, Li M, Knyaz C, Tamura K. 2018. MEGA X: molecular evolutionary genetics analysis across computing platforms. *Molecular Biology and Evolution* 35:1547–1549

[42] Shen Q, Zhang L, Liao Z, Wang S, Yan T, et al. 2018. The genome of *Artemisia annua* provides insight into the evolution of Asteraceae family and artemisinin biosynthesis. *Molecular Plant* 11:776–788

[43] Yan T, Li L, Xie L, Chen M, Shen Q, et al. 2018. A novel HD-ZIP IV/MIXTA complex promotes glandular trichome initiation and cuticle development in *Artemisia annua*. *New Phytologist* 218:567–578

[44] Zhang L, Jing F, Li F, Li M, Wang Y, et al. 2009. Development of transgenic *Artemisia annua* (Chinese wormwood) plants with an enhanced content of artemisinin, an effective anti-malarial drug, by hairpin-RNA-mediated gene silencing. *Biotechnology and Applied Biochemistry* 52:199–207

[45] Liu H, He W, Yao X, Yan X, Wang X, et al. 2023. The light- and jasmonic acid-induced *AaMYB108-like* positive regulates the initiation of glandular secretory trichome in *Artemisia annua* L. *International Journal of Molecular Sciences* 24:12929

[46] Boutrot F, Chantret N, Gautier MF. 2008. Genome-wide analysis of the rice and Arabidopsis *non-specific lipid transfer protein* (*nsLtp*) gene families and identification of wheat *nsLtp* genes by EST data mining. *BMC Genomics* 9:86

[47] Li J, Gao G, Xu K, Chen B, Yan G, et al. 2014. Genome-wide survey and expression analysis of the putative non-specific lipid transfer proteins in *Brassica rapa* L. *PLoS One* 9:e84556

[48] Chew W, Hrmova M, Lopato S. 2013. Role of homeodomain leucine zipper (HD-Zip) IV transcription factors in plant development and plant protection from deleterious environmental factors. *International Journal of Molecular Sciences* 14:8122–8147

[49] Wang B, Kashkooli AB, Sallets A, Ting HM, de Ruijter NCA, et al. 2016. Transient production of artemisinin in *Nicotiana benthamiana* is boosted by a specific lipid transfer protein from *A. annua*. *Metabolic Engineering* 38:159–169

[50] Hoh F, Pons JL, Gautier MF, de Lamotte F, Dumas C. 2005. Structure of a liganded type 2 non-specific lipid-transfer protein from wheat and the molecular basis of lipid binding. *Acta Crystallographica Section D Structural Biology* 61:397–406

[51] Jain A, Salunke DM. 2017. Crystal structure of nonspecific lipid transfer protein from *Solanum melongena*. *Proteins: Structure, Function, and Bioinformatics* 85:1820–1830

[52] Madni ZK, Tripathi SK, Salunke DM. 2020. Structural insights into the lipid transfer mechanism of a non-specific lipid transfer protein. *The Plant Journal* 102:340–352

[53] Waigmann E, Turner A, Peart J, Roberts K, Zambryski P. 1997.Ultrastructural analysis of leaf trichome plasmodesmata reveals major differences from mesophyll plasmodesmata. *Planta* 203:75–84

[54] Gossart N, Berhin A, Sergeant K, Alam I, André C, et al. 2023. Engineering *Nicotiana tabacum* trichomes for triterpenic acid production. *Plant Science* 328:111573

[55] Li J, Hu H, Fu H, Li J, Zeng T, et al. 2024. Exploring the co-operativity of secretory structures for defense and pollination in flowering plants. *Planta* 259:41

[56] Liu D, Dou W, Song H, Deng H, Tian Z, et al. 2025. Insights into the functional mechanism of the non-specific lipid transfer protein nsLTP in *Kalanchoe fedtschenkoi* (*Lavender scallops*). *Protein Expression and Purification* 226:106607

[57] Chen Q, Li L, Qi X, Fang H, Yu X, et al. 2023. The non-specific lipid transfer protein McLTPII.9 of *Mentha canadensis* is involved in peltate glandular trichome density and volatile compound metabolism. *Frontiers in Plant Science* 14:1188922

[58] Kashkooli AB, van Dijk ADJ, Bouwmeester H, van der Krol A. 2023. Individual lipid transfer proteins from *Tanacetum parthenium* show different specificity for extracellular accumulation of sesquiterpenes. *Plant Molecular Biology* 111:153–166

[59] Chatzopoulou FM, Makris AM, Argiriou A, Degenhardt J, Kanellis AK. 2010. EST analysis and annotation of transcripts derived from a trichome-specific cDNA library from *Salvia fruticosa*. *Plant Cell Reports* 29:523–534

[60] Wang G, Tian L, Aziz N, Broun P, Dai X, et al. 2008. Terpene biosynthesis in glandular trichomes of hop. *Plant Physiology* 148:1254–1266

[61] Falara V, Fotopoulos V, Margaritis T, Anastasaki T, Pateraki I, et al. 2008. Transcriptome analysis approaches for the isolation of trichome-specific genes from the medicinal plant *Cistus creticus* subsp. *creticus*. *Plant Molecular Biology* 68:633–651

[62] Bertea CM, Voster A, Verstappen FWA, Maffei M, Beekwilder J, et al. 2006. Isoprenoid biosynthesis in *Artemisia annua*: cloning and heterologous expression of a germacrene A synthase from a glandular trichome cDNA library. *Archives of Biochemistry and Biophysics* 448:3–12

[63] Aziz N, Paiva NL, May GD, Dixon RA. 2005. Transcriptome analysis of alfalfa glandular trichomes. *Planta* 221:28–38

[64] Gang DR, Wang J, Dudareva N, Nam KH, Simon JE, et al. 2001. An investigation of the storage and biosynthesis of phenylpropenes in sweet basil. *Plant Physiology* 125:539–555

[65] Lange BM, Wildung MR, Stauber EJ, Sanchez C, Pouchnik D, et al. 2000. Probing essential oil biosynthesis and secretion by functional evaluation of expressed sequence tags from mint glandular trichomes. *Proceedings of the National Academy of Sciences of the United States of America* 97:2934–2939

[66] Tsuboi S, Osafune T, Tsugeki R, Nishimura M, Yamada M. 1992. Nonspecific lipid transfer protein in castor bean cotyledon cells: subcellular localization and a possible role in lipid metabolism. *The Journal of Biochemistry* 111:500–508

[67] Salminen TA, Blomqvist K, Edqvist J. 2016. Lipid transfer proteins: classification, nomenclature, structure, and function. *Planta* 244:971–997

[68] Turchi L, Baima S, Morelli G, Ruberti I. 2015. Interplay of HD-Zip II and III transcription factors in auxin-regulated plant development. *Journal of Experimental Botany* 66:5043–5053

[69] Wu M, Bian X, Hu S, Huang B, Shen J, et al. 2024. A gradient of the HD-Zip regulator Woolly regulates multicellular trichome morphogenesis in tomato. *The Plant Cell* 36:2375–2392

[70] Verma S, Attuluri VPS, Robert HS. 2022. Transcriptional control of Arabidopsis seed development. *Planta* 255:90